Heterogeneous Sensitivity to Src Inhibitors in Oral Squamous Cell Carcinoma and Its Implications for Combination Therapy with Cisplatin

Yuri Ofusa, Tadahide Noguchi, Hiroaki Mizukami & Kenji Ohba

1. Division of Genetic Therapeutics, Center for Molecular Medicine, Jichi Medical University, Shimotsuke, Tochigi, Japan

2. Department of Dentistry, Oral and Maxillofacial Surgery, Jichi Medical University, Shimotsuke, Tochigi, Japan

Running title; Suppression of oral cancers by Src inhibitors

Competing interests

The authors declare no competing financial interests.

This work was supported by AMED under Grant Number, JP23bm1323001, JMU Graduate Student Start-Up Award, and JST SPRING, Grant Number JPMJSP2183.

* Correspondence should be addressed to K.O. (ohbak@jichi.ac.jp)

3311-1 Yakushiji, Shimotsuke, Tochigi, 329-0498, Japan

Tel: +81-258-58-7402, Fax: +81-258-44-8675

email: ohbak@jichi.ac.jp

Abstract

Purpose:

Treatment options of advanced oral squamous cell carcinomas (OSCC) are limited, and cisplatin toxicity and drug resistance are major clinical issues. Src is a central kinase that integrates multiple oncogenic pathways and a promising therapeutic target. However, Src inhibitors have shown suboptimal efficacy as monotherapies and their sensitivity in OSCC remains elusive.

Experimental Design:

We examined the activation of major oncogenic signaling pathways and the antitumor effects of six Src inhibitors (dasatinib, ponatinib, vandetanib, saracatinib, PP2, bosutinib) in seven human OSCC cell lines (HSC-2, HSC-3, HSC-4, SAS, HO-1-u-1, CAL27, SCC-25). BALB/cAJcl nu/nu mice bearing CAL27 xenografts received dasatinib (30 mg/kg, intraperitoneally, daily), bosutinib (50 mg/kg, intraperitoneally, daily), cisplatin (2 mg/kg or 4 mg/kg, intraperitoneally, weekly), or combinations. Tumor volume, bioluminescence imaging, and body weight were monitored for 17 or 21 days, followed by histopathological assessment.

Results:

The activation of the key pathways, including Src and MAPK, considerably differed among the cell lines and was linked to heterogeneous sensitivity to Src inhibitors. Effective growth suppression required Src dephosphorylation and downstream MAPK pathway inhibition, which vary depending on the cell line. Additionally, combination treatment with a Src inhibitor and cisplatin showed additive antitumor effects, allowing the reduction of cisplatin doses by half without efficacy loss. Notably, dasatinib alone and in combination with cisplatin decreased tumor burden with characteristic internal tumor death *in vivo*.

Conclusions:

These findings elucidate Src signaling dependency on OSCC and the potential of Src inhibition to decrease cisplatin toxicity, paving way for Src targeted therapeutic strategies.

Introduction

Oral squamous cell carcinoma (OSCC) is a malignant disease on the mucosal surfaces of the tongue, gingiva, and lips, and is the most common subtype of head and neck malignancy(1). Approximately 390,000 new cases of OSCC were reported worldwide in 2022, and the rate of increase is predicted to reach nearly 60% by 2050, according to the Global Cancer Observatory (2).

Almost 60% of patients with oral cancer are diagnosed at advanced stages (stage III–IV), with a 5-year survival rate of less 60%(3–6). Managing patients with advanced cancer requires multimodal treatment including surgery, radiotherapy, and chemotherapy(6). Although multidisciplinary therapy is effective for managing advanced cancer, it is quite invasive, resulting in treatment-related cosmetic and functional impairments such as dysphagia and speech difficulties, which considerably compromise the quality of life(QOL) patients (7). Moreover, 10–50% of patients experience local recurrence or distant metastasis following initial therapy, and only a minority are eligible for salvage surgery or radiotherapy(8–10). Palliative or supportive care is the last option for most patients with recurrent or metastatic cancer, with a median survival of 4–9 months(3,11). Thus, improving the prognosis and QOL of patients with OSCC remains an urgent clinical challenge.

Systemic chemotherapy plays a key role, especially in patients with recurrent or metastatic cancer. Cisplatin is the standard systemic therapy in definitive chemoradiotherapy and recurrent/metastatic settings. However, owing to severe toxicities, few patients with adequate performance status (PS) can be prescribed cisplatin(12). No alternative systemic therapy with efficacy comparable to that of cisplatin has been established for patients ineligible due to age, comorbidities, or poor PS(3). In addition, cisplatin resistance occurs in approximately 30–40% of patients with OSCC, substantially limiting its therapeutic effect(13). Therefore, drugs that decrease cytotoxicity and overcome cisplatin resistance are necessary.

Several studies have explored the use of cisplatin substitutes. While carboplatin shows lower toxicity than cisplatin, its antitumor activity is inferior to cisplatin at equivalent doses(14). Cetuximab is the only molecular-targeted drug approved for OSCC. However, it has not shown clear superiority over cisplatin yet (15). Even though immune checkpoint inhibitors such as pembrolizumab and nivolumab have recently been approved for treating recurrent/metastatic OSCC, their response rates are limited to approximately 10–20%(16,17). The identification of new effective therapeutic agents for OSCC is a crucial unmet clinical need.

90 A central non-receptor tyrosine kinase within the Src family of kinases (SFKs), c-Src
91 (hereafter, Src), regulates multiple cellular processes involved in malignant progression,
92 including proliferation, survival, migration, invasion and angiogenesis(18). Src
93 hyperactivation has been noted in solid tumors, including breast, colorectal, pancreatic,
94 ovarian, gastric, esophageal, and lung cancers and is strongly liked to poor prognosis(19).
95 This indicates that Src inhibitors are potential candidates for cancer chemotherapy. Src
96 activation is correlated with poor clinical outcomes and invasive and metastatic potential
97 in head and neck squamous cell carcinoma (HNSCC)(20). Particularly, in OSCC, high
98 Src expression is markedly linked to tumor size, lymph node metastasis, advanced stage
99 and recurrence, and has been identified as an independent prognostic factor. This suggests
100 that Src plays a crucial role in OSCC progression(21).
101 Preclinical studies have revealed that FDA-approved Src inhibitors, including dasatinib
102 and saracatinib, suppress proliferation, migration and invasion, and induce apoptosis in
103 HNSCC/OSCC models(19,22,23). Despite these promising results, Src inhibitors have
104 demonstrated suboptimal efficacy as monotherapies in clinical trials(24,25). Possible
105 mechanisms behind this discrepancy include the non-lethal nature of Src inhibition in
106 HNSCC/OSCC cells, compensatory activation of alternative pathways, such as
107 PI3K/AKT and STAT3(22,26), and variations in EMT status or cell adhesion molecules

108 that affect drug sensitivity(27,28). Substantial efforts have been directed toward
109 elucidating the mechanisms of action of Src inhibitors and identifying biomarkers that
110 predict the therapeutic response in lung, colorectal, and breast cancers, where oncogenic
111 driver mutations are well characterized. However, the molecular determinants of Src
112 inhibitor sensitivity in OSCC remain elusive.

113 HNSCC/OSCC is characterized by profound molecular heterogeneity, with distinct
114 dependencies on kinases, such as EGFR, EPHA2, AURKA, WEE1, and JAK1 across
115 various cell lines(29). This heterogeneity suggests that sensitivity to Src inhibition may
116 markedly differ among the OSCCs. However, there is no report systematically
117 investigating Src inhibitor sensitivity in OSCC, especially using animal models.
118 Moreover, recent the combined effects of Src inhibitors and cisplatin may provide a
119 strategy to overcome cisplatin resistance and decrease toxicity in gastric cancer and
120 tubular epithelial cells(30,31).

121 Based on this evidence, we sought to reassess the therapeutic potential of Src inhibition
122 in OSCC and generate foundational insights that may guide the optimization of future
123 treatment strategies. We analyzed Src inhibitor sensitivity across multiple OSCC cell lines
124 and a mouse model and assessed the therapeutic effect of combining Src inhibition with
125 cisplatin.

126 **Materials and Methods**

127 **Cell culture**

128 Seven human OSCC cell lines were utilized. RIKEN BRC (Tsukuba, Japan) provided
129 HSC-2 (RCB1945), HSC-3 (RCB1975), HSC-4 (RCB1902), SAS (RCB1974), and HO-
130 1-u-1 (RCB2102). CAL27 (CRL-2095) and SCC-25 (CRL-1628) cells were purchased
131 from the American Type Culture Collection (ATCC, VA). HSC-2 and HSC-3 cells were
132 maintained in E-MEM (051-07615, Wako, Osaka, Japan). HSC-4, SAS, and HO-1-u-1
133 cells were maintained in RPMI-1640 (189-02023, Wako). Furthermore, CAL27 cells
134 were maintained in high-glucose DMEM supplemented with L-glutamine, phenol red,
135 and sodium pyruvate (041-30081, Wako). SCC-25 cells were maintained in a 1:1
136 mixture of DMEM and Ham's F-12 medium containing L-glutamine, phenol red,
137 HEPES, and sodium pyruvate (042-30555, Wako) supplemented with 400 ng/mL
138 hydrocortisone. All mediums cultivating cells mentioned above were further
139 supplemented with 10% fetal bovine serum (Gibco, CA) and 1% penicillin-
140 streptomycin (100×, Wako), and cells were maintained at 37°C in a humidified
141 atmosphere containing 5% CO_2 before use. All cell lines used were cultured within
142 three months of the second passage.

143

144 **Reagents**

145 Src inhibitors used in this study are as follows. Dasatinib (SML2589, TCI TC-I 201,
146 and D5949) was obtained from Sigma-Aldrich. Ponatinib (AMBH303C5EAB),
147 vandetanib (SML2983), and saracatinib (SML3195) were purchased from Sigma-
148 Aldrich. Additionally, PP2 (529573) was purchased from Calbiochem (MA). Bosutinib
149 (T0152) was obtained from TargetMol, MA. The Src inhibitors were dissolved in
150 dimethyl sulfoxide (DMSO). Cisplatin (033-20091) was obtained from Wako and was
151 dissolved in 0.9% NaCl.

152

153 **Antibodies**

154 The following primary antibodies were utilized: p53 (7F5) Rabbit mAb (#2527),
155 Phospho-p53 (Ser15) Antibody (#9284), Src (32G6) Rabbit mAb (#2123), Phospho-Src
156 Family (Tyr416) (D49G4) Rabbit mAb (#6943), Ras (D2C1) Rabbit mAb (#8955), p38
157 MAPK (D13E1) XP Rabbit mAb (#8690), Phospho-p38 MAPK (Thr180/Tyr182)
158 (D3F9) XP Rabbit mAb (#4511), p44/42 MAPK (Erk1/2) (137F5) Rabbit mAb (#4695),
159 Phospho-p44/42 MAPK (Erk1/2) (Thr202/Tyr204) (D13.14.4E) XP Rabbit mAb
160 (#4370), SAPK/JNK Antibody (#9252), Phospho-SAPK/JNK (Thr183/Tyr185) (81E11)
161 Rabbit mAb (#4668), and β-Actin Antibody (#4967) (all from Cell Signaling

162 Technology, MA). The K-Ras Monoclonal Antibody (9.13) was purchased from

163 Invitrogen (Carlsbad, CA). For detection, Anti-rabbit IgG, HRP-linked Antibody (Cell

164 Signaling Technology) was used for all primary antibodies except K-Ras and β-actin,

165 for which HRP-conjugated anti-mouse IgG secondary antibodies (Cell Signaling

166 Technology) were used.

167

168 **Western blotting**

169 HSC-2, HSC-3, HSC-4, SAS, HO-1-u-1, CAL27, and SCC-25 cells were lysed using

170 M-PER Mammalian Protein Extraction Reagent (Thermo Fisher Scientific, NY)

171 supplemented with 10× Complete protease inhibitor and 10× PhosSTOP phosphatase

172 inhibitor (Roche, Basel, Switzerland), mixed with an equal volume of 2× sodium

173 dodecyl sulfate (SDS) buffer, and boiled at 90 °C for 10 min. Proteins were separated

174 using SDS-polyacrylamide gel electrophoresis (PAGE) and transferred onto

175 polyvinylidene fluoride membranes. Membranes were blocked with Every Blot

176 Blocking Buffer (Bio-Rad Laboratories, Hercules, CA) and incubated with primary

177 antibodies for 1 h at 25 ℃. After washing with Tris-buffered saline containing 0.1%

178 Tween-20 (TBS-T), the membranes were incubated with secondary antibodies for 1 h at

179 25 ℃. Protein bands were visualized using Clarity Western ECL Substrate (Bio-Rad

180 Laboratories) and imaged using a ChemiDoc Toch MP Imaging System (Bio-Rad
181 Laboratories).
182 For phosphorylation analysis following Src inhibitor treatment, HSC-2, HSC-3, HSC-4,
183 SAS, HO-1-u-1, CAL27, and SCC-25 cells were treated with dasatinib, ponatinib,
184 vandetanib, or bosutinib for 18 h. The cells were seeded in 12 well plates at densities
185 that yielded approximately 80% confluence at the treatment time. Supplementary Table
186 S1 provides the concentrations utilized for each cell line. Cells were harvested using the
187 same lysis procedure described above, and protein samples were subjected to SDS-
188 PAGE and western blotting, as previously described. The following primary antibodies
189 were used: Phospho-Src Family (Tyr416) (D49G4) Rabbit mAb (#6943), Phospho-
190 p44/42 MAPK (Erk1/2) (Thr202/Tyr204) (D13.14.4E) XP Rabbit mAb (#4370),
191 Phospho-p38 MAPK (Thr180/Tyr182) (D3F9) XP Rabbit mAb (#4511), and Phospho-
192 SAPK/JNK (Thr183/Tyr185) (81E11) Rabbit mAb (#4668) (all from Cell Signaling
193 Technology). Detection and imaging were conducted as previously described.
194
195 **Cell viability assays**
196 Cell viability was evaluated using the CellTiter-Glo® 2.0 Reagent (Promega, WI). Cells
197 were seeded into Costar 96-well flat white plates (3917, Costar, NY) at the following

198 densities: HSC-2 (0.8×10^4), HSC-3 (1.0×10^4), HSC-4 (0.8×10^4), SAS (2.0×10^4),

199 HO-1-u-1 (1.5×10^4), CAL27 (1.5×10^4), and SCC-25 (0.7×10^4) cells per well, and

200 allowed to adhere overnight. HSC-2, HSC-3, HSC-4, SAS, HO-1-u-1, CAL27, and

201 SCC-25 cells were treated with the Src inhibitors dasatinib (100 nM), ponatinib (2 μM),

202 vandetanib (10 μM), saracatinib (5 μM), PP2 (50 μM), bosutinib (5 μM), or cisplatin

203 (10 μM) for 72 h. All compounds were diluted in a culture medium at the final

204 concentration of DMSO with 1%, and cell viability was calculated relative to the 1%

205 DMSO control. Following drug treatment, CellTiter-Glo® 2.0 reagent was added at a

206 1:1 ratio to the culture medium, mixed for 2 min on an orbital shaker and incubated for

207 10 min at 25 ℃ to stabilize the luminescent signal. The luminescence was measured

208 using a Tecan Spark microplate reader (TECAN, Männedorf, Switzerland). All

209 experiments were conducted in triplicates (n = 3).

210 For IC_{50} determination, cells were seeded into Costar 96-well flat white plates (3917,

211 Costar) at the same densities described above for each cell line and allowed to adhere

212 overnight. Cells were subsequently treated with serial dilutions of dasatinib, ponatinib,

213 saracatinib, or bosutinib for 36 h. Cell viability was measured using the CellTiter-Glo®

214 2.0 Reagent (Promega) as described above. IC_{50} values were calculated from dose-

215 response curves using nonlinear regression in R (version 4.5.2). All experiments were
216 conducted in triplicates (n = 3).
217 For combination treatment assays, cell viability was evaluated using the CellTiter-Glo®
218 2.0 Reagent (Promega). Cells were seeded in Costar 96-well flat white plates (3917,
219 Costar) at the cell line-specific densities described above and allowed to adhere
220 overnight. Cells were treated with cisplatin (10 μM or 5 μM), each Src inhibitor alone,
221 or their combinations for 36 h. Supplementary Table S2 provides the Src inhibitor
222 concentrations used for each cell line. All compounds were diluted in the culture
223 medium to a final concentration of DMSO (1%), and cell viability was calculated
224 relative to the 1% DMSO control. Luminescence was measured using a Tecan Spark
225 microplate reader (TECAN). All experiments were performed in triplicates (n = 3).
226
227 **Lentiviral production and generation of Renilla luciferase (RLuc)-expressing**
228 **CAL27 cells**
229 RLuc-expressing CAL27 (CAL27-Rluc) cells were generated by infecting parental
230 CAL27 cells with lentiviral particles produced by HEK293T cells. Lentiviruses were
231 produced by co transfecting HEK293T cells with the packaging plasmids pCMV-VSVG
232 -RSV-Rev (1 μg/μL) and pCAG-HIVgp-RRE (1 μg/μL), together with the transfer

233 vector CSII-EGFP-P2A-RLuc-IRES-Bsd at a ratio of 1:1:2. Viral infection of CAL27
234 cells was conducted in the presence of polybrene at a 10 μg/mL final concentration.
235 Seven independent CAL27-Rluc clones were established following infection and
236 blasticidin selection. RLuc activity in each clone was confirmed using EnduRen live
237 cell Renilla luciferase substrate (Promega) according to the manufacturer's instructions.
238 The drug responsiveness of the clones was assessed 36 h following treatment with Src
239 inhibitors and cisplatin under the same conditions used for the Cell-Titer Glo® assay.
240 Supplementary Fig. 1 shows the detailed screening results for the seven clones.
241
242 **Animal experiments**
243 CAL27-Rluc cells (clone 7; 2×10^7 cells/mouse) were subcutaneously implanted into
244 the right flank of 5-week-old male BALB/cAJcl nu/nu mice (CLEA Japan, Tokyo,
245 Japan). The mice were kept in a 12-hour light-dark cycle and were given free access to
246 food and water. Three days following implantation, the mice were randomly assigned to
247 six treatment groups based on their body weight (n = 5-6 in each group): vehicle control
248 (DMSO), dasatinib alone (30 mg/kg), cisplatin alone (4 mg/kg), cisplatin alone (2
249 mg/kg), dasatinib (30 mg/kg) + cisplatin (4 mg/kg), and dasatinib (30 mg/kg) + cisplatin
250 (2 mg/kg). Dasatinib and DMSO were dissolved in 10 mM Tris-HCl (pH 7.4), and

251 cisplatin was dissolved in 0.9% NaCl. All drugs were intraperitoneally administered at a
252 volume of 100 μL per mouse. Dasatinib and DMSO were administered once daily,
253 whereas cisplatin was administered once weekly for two consecutive weeks. This
254 dosing schedule was designed to approximate the clinical dosing frequencies in humans.
255 In a separate experiment conducted under identical implantation and monitoring
256 conditions, the mice were assigned to three groups: vehicle control (DMSO), dasatinib
257 alone (30 mg/kg), and bosutinib alone (50 mg/kg). Bosutinib was dissolved in 10 mM
258 Tris HCl (pH 7.4) and intraperitoneally administered once daily at a volume of 100 μL
259 per mouse, following the same dosing schedule as in the dasatinib experiment.
260 To detect Renilla luciferase activity, ViviRen™ In Vivo Renilla Luciferase Substrate
261 (Promega) was dissolved in dimethyl sulfoxide at 10 mg/mL to prepare a stock solution,
262 which was subsequently diluted 1,000-fold in PBS containing 0.1% bovine serum
263 albumin. A total of 100 μL (1 mg) of the diluted substrate was intravenously
264 administered. Mice were anesthetized with isoflurane, and bioluminescence imaging
265 was conducted using an IVIS system. Bioluminescence signals were quantified 10 min
266 following ViviRen injection according to the manufacturer's instructions(32). IVIS
267 image analysis was performed on days 5, 7, 10, and 13 after subcutaneous tumor
268 transplantation and on days 7, 13, and 20, respectively.

269 Tumor volumes were measured using calipers and calculated as $L \times W^2 \times 0.52$. Body
270 weight was monitored every 2-3 d throughout the treatment period. At the end of the
271 treatment, the mice were perfusion-fixed, and the tumor, kidney, and liver were
272 harvested (N＝5-6). All animal experiments were conducted in accordance with the
273 Animal Experimentation Regulations of the Jichi Medical University. The Institutional
274 Animal Care and Use Committee of Jichi Medical University reviewed and approved
275 the study protocol. The study subsequently received final authorization from the
276 University President.
277
278 **Hematoxylin and Eosin (H&E) staining**
279 Excised tumor, kidney, and liver tissues were fixed in 1% paraformaldehyde at 4 °C
280 overnight. The tissues were subsequently cryoprotected by sequential incubation in 10%
281 sucrose/PBS and 20% sucrose/PBS at 4 °C, each for 24 h. After cryoprotection, the
282 tissues were embedded in OCT compound (Sakura Finetek, Tokyo, Japan) and snap-
283 frozen in liquid nitrogen. Frozen blocks were sectioned at 8 μm thickness, and the
284 sections were stained with H&E using standard procedures. The sections were post-
285 fixed in 2% paraformaldehyde, stained with hematoxylin, rinsed under running tap
286 water, counterstained with eosin, dehydrated using graded ethanol, cleared in xylene,

287 and mounted with coverslips. Histological images were obtained using a light

288 microscope.

289

290 **Statistical analysis**

291 No statistical methods were used to predetermine sample size. Mouse studies were

292 randomized; however, the investigators were not blinded to group allocation during the

293 experiments or outcome assessment. Western blot analysis was independently

294 performed three times. IC_{50} values for the Src inhibitors were calculated from three

295 independent CellTiter-Glo assays, and mean ± standard deviation (SD) was obtained

296 using Microsoft Excel. For *in vitro* combination assays of the Src inhibitors and

297 cisplatin, data are presented as mean ± SD from n = 3, and P values were calculated

298 using paired t-tests in Microsoft Excel. Statistical significance was defined as follows: p

299 < 0.01 **, $p < 0.05$ *, and $p \geqq 0.05$ ns.

300 For *in vivo* experiments, tumor volume and body weight were analyzed using data from

301 surviving mice at each time point (n = 5–6), and mean ± SD was calculated using R

302 (version 4.5.2).

303

304 **Results**

305 **OSCC cell lines show substantial heterogeneity in the activation of major oncogenic**

306 **signaling pathways**

307 Cancer develops through the accumulation of genetic and epigenetic changes in

308 oncogenic signaling pathways, eventually resulting in the acquisition of malignant

309 phenotypes(33). In OSCC, p53 mutations frequently occur(34), and multiple oncogenic

310 pathways including EGFR, PI3K/AKT/mTOR, JAK/STAT, MET, Wnt/β-catenin and

311 RAS/RAF/MAPK are aberrantly activated and contribute to tumor progression(35).

312 Besides, the activation of MAPK signaling (ERK1/2, JNK, p38, and ERK5) is involved

313 in HNSCC oncogenicity(35). These observations suggest that the activity of signaling

314 networks in the OSCC cell lines may markedly vary.

315 To test this hypothesis, we investigated the phosphorylation status of key signaling

316 molecules by western blotting (Fig. 1A). HSC-4 and CAL27 revealed increased protein

317 levels of p53 and phosphor-p53 (p-p53) (Ser15). Total Src expression was consistent in

318 all cell lines; however, its active form, phospho-Src (p-Src) (Tyr416), was detected in all

319 cell lines except HSC-3 and SCC-25. K-Ras expression was augmented in SAS, HO-1-

320 u-1, and CAL27, and the discrepancy between Ras expression and activation in HSC-2

321 and SAS suggested N-Ras or H-Ras activation. Within the MAPK pathway, all seven

322 cell lines exhibited strong p38 and ERK1/2 activation, as shown by elevated
323 phosphorylation levels (p-p38 and p-ERK1/2), which closely paralleled the activation
324 pattern of p-Src (Tyr416). This concordant activation pattern suggested that Src activity
325 was closely associated with downstream MAPK signaling in the OSCC cells.
326 Contrastingly, SAPK/JNK expression was relatively high in HSC-2, SAS, HO-1-u-1,
327 and CAL27, whereas enhanced SAPK/JNK phosphorylation was only noted in SAS and
328 HO-1-u-1, indicating a more selective activation profile. Thus, broadly activated Src,
329 together with the downstream signaling activation patterns noted in the OSCC cell lines,
330 could be a promising target for chemotherapy in OSCCs.

Figure 1 Src activity and its inhibitory effect of tumor growth by specific inhibitors in various oral cancer cell lines

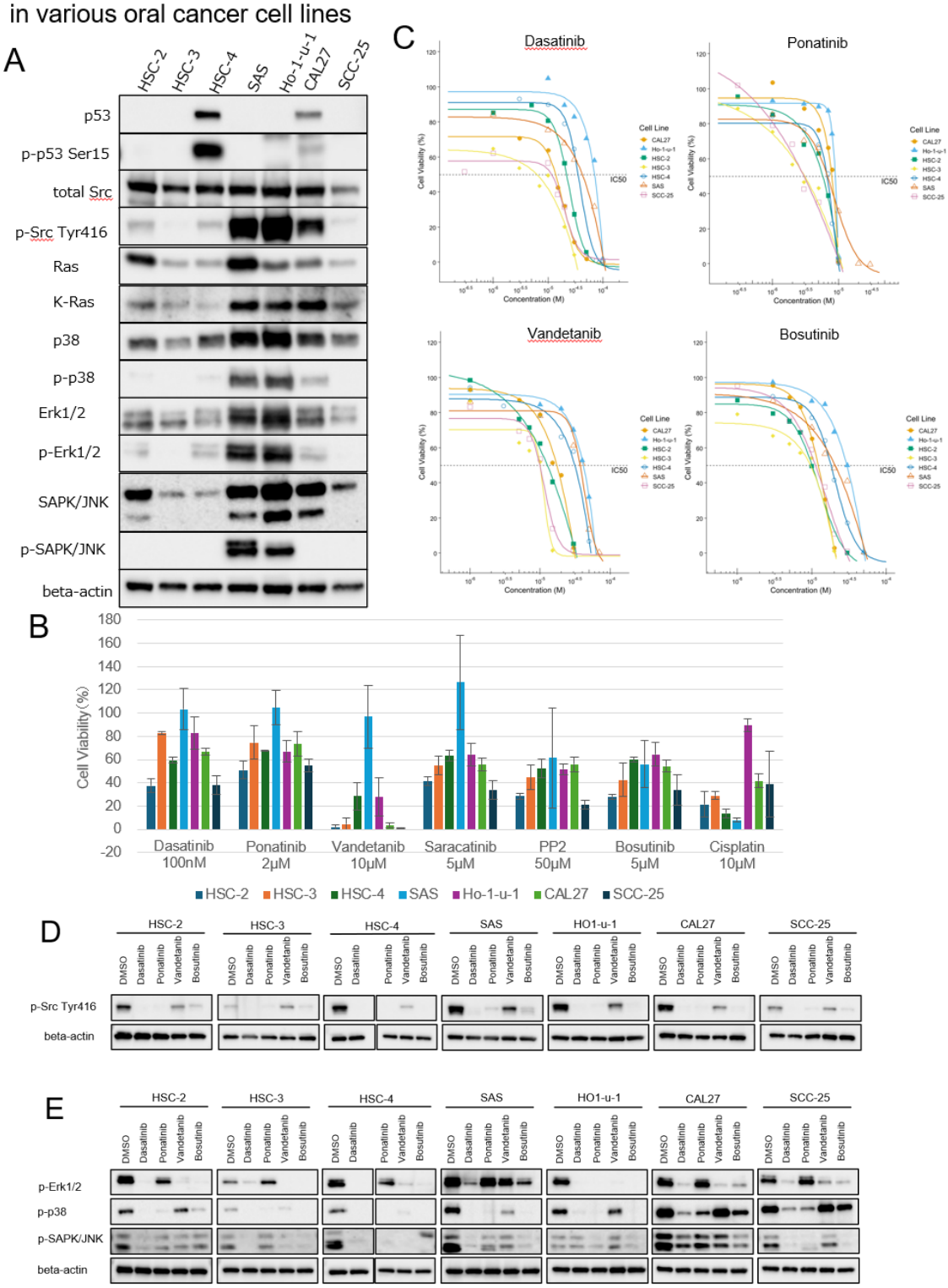

331

332 **Src activity and its inhibitory effect of tumor growth by specific inhibitors in**

333 **different oral cancer cell lines**

334 Some Src inhibitors have already been approved for clinical cancer therapies(19,22,23),

335 suggesting that these Src inhibitors can be easily utilized for oral cancers if their

336 anticancer effect is prospective. Next, we evaluated the sensitivity of the OSCC cell lines

337 to FDA-approved Src inhibitors. Despite PP2 is not FDA-approved, it was included for

338 comparison because it is frequently used as a research-grade Src inhibitor. Treatment of

339 seven OSCC cell lines with each Src inhibitor at concentrations close to their mean IC_{50}

340 showed variation in cell line viability (Fig. 1B). HSC-2 and SCC-25 were broadly

341 sensitive to all the inhibitors tested, whereas SAS showed lower sensitivity (Fig. 1B).

342 Comparison of the IC_{50} values obtained following 36 h of treatment indicated differences

343 between the inhibitors (Table 1, Fig. 1C). Dasatinib, vandetanib, saracatinib, and PP2

344 revealed pronounced variability in their IC_{50} values across cell lines. In contrast, ponatinib

345 and bosutinib showed broad antitumor effects with less variability in cell lines (Table 1,

346 Fig. 1C). Notably, HO-1-u-1 showed resistance to cisplatin. Thus, OSCC cell lines show

347 distinct pharmacological vulnerabilities resulting from the differences in the activating

348 pathways for Src signaling.

349 We examined p-Src (Tyr416) levels 18 h following inhibitor treatment to determine

350 whether the differences in antitumor activity were attributable to the degree of Src

351 inhibition (Fig. 1D). All inhibitors suppressed Src activation, although vandetanib

352 exhibited a relatively weaker inhibition. This effect was especially modest in SAS and

353 HO-1-u-1, which is consistent with their reduced sensitivity (Figs. 1B and 1C).

Table 1 The half maximal inhibitory concentration (IC50) of Src inhibitors in various oral cancer cell lines after 36 h of treatment

	Dasatinib	Ponatinib	Vandetanib	Saracatinib	PP2	Bosutinib	Cisplatin
HSC-2	0.1 μM	2 μM	5 μM	5 μM	50 μM	5 μM	10 μM
HSC-3	10 μM	2 μM	8 μM	10 μM	100~250 μM	5 μM	1~5 μM
HSC-4	25 μM	5~10 μM	25 μM	100 μM	600 μM	15 μM	10 μM
SAS	10 μM	5~10 μM	50 μM	100 μM	＞600 μM	25 μM	10 μM
Ho-1-u-1	50 μM	5~10 μM	25 μM	50~100 μM	＞600 μM	25 μM	＞50 μM
CAL27	10~25 μM	5~10 μM	10~50 μM	25 μM	＞600 μM	15 μM	10 μM
SCC-25	10 μM	2~5 μM	8~10 μM	50 μM	200 μM	10 μM	10 μM

354 We further assessed whether Src inhibition suppressed the phosphorylation of MAPK

355 subpathways (ERK1/2, p38, and JNK; Fig. 1E). Dasatinib completely suppressed all

356 MAPK components in all the cell lines. Ponatinib completely inhibited p38 and largely

357 inhibited JNK phosphorylation, whereas the suppression was partial in CAL27.

358 Vandetanib inhibited distinct MAPK components, depending on the cell line used.

359 Bosutinib typically inhibited the phosphorylation of all MAPK components except ERK

360 in SAS and p38 in SCC-25. Thus, while the pathway associated with the upregulation of

361 Src varies in cells, different inhibitors targeting Src activity are effective in suppressing
362 the growth of OSCC cell lines.
363 Taken together, these results suggest that the activation status of major signaling pathways
364 involving Src significantly differs across the OSCC cell lines and that such molecular
365 differences may underlie the observed variation in sensitivity to Src inhibitors.
366
367 **Tumor inhibitory effect by combination therapy using cisplatin and Src inhibitors**
368 OSCC cell lines showed considerable heterogeneity such as variable susceptibilities to
369 Src inhibitors and cisplatin (Fig. 1). Next, we assessed the combinatorial effects of Src
370 inhibitors with cisplatin at 10 μM and 5 μM (Fig. 2).
371 Compared with cisplatin at 10 μM, Src inhibitors alone revealed equal or lower antitumor
372 activity in most OSCC cell lines, except for HO-1-u-1 and SCC-25, indicating that Src
373 inhibition was effective in the OSCC cell lines. The combination treatment showed
374 additive effects in HSC-3, HSC-4, CAL27, and SCC-25, especially with dasatinib and
375 bosutinib, and these effects increased in a cisplatin dose-dependent manner. Although
376 cisplatin at 5 μM alone showed limited activity, its combination with Src inhibitors
377 produced antitumor effects comparable to or more for 10 μM cisplatin alone in HSC-4,
378 CAL27, and SCC-25.

379 On the other hand, cisplatin-resistant HO-1-u-1 responded better to Src inhibitors alone
380 than to cisplatin, and no enhancement was noted with the combination treatment. This
381 indicates that the efficacy of Src-cisplatin combination therapy may be determined by the
382 intrinsic cisplatin sensitivity of each OSCC cell line and its degree of dependence on Src
383 signaling.
384 These results suggest that combining Src inhibitors with cisplatin may reduce the cisplatin
385 dose to half of the standard *in vitro* therapeutic concentration while maintaining its
386 efficacy in cisplatin-sensitive OSCC.
387
388
389
390
391

Figure 2 The tumor inhibitory effect by combination therapy using Cisplatin and Src inhibitor

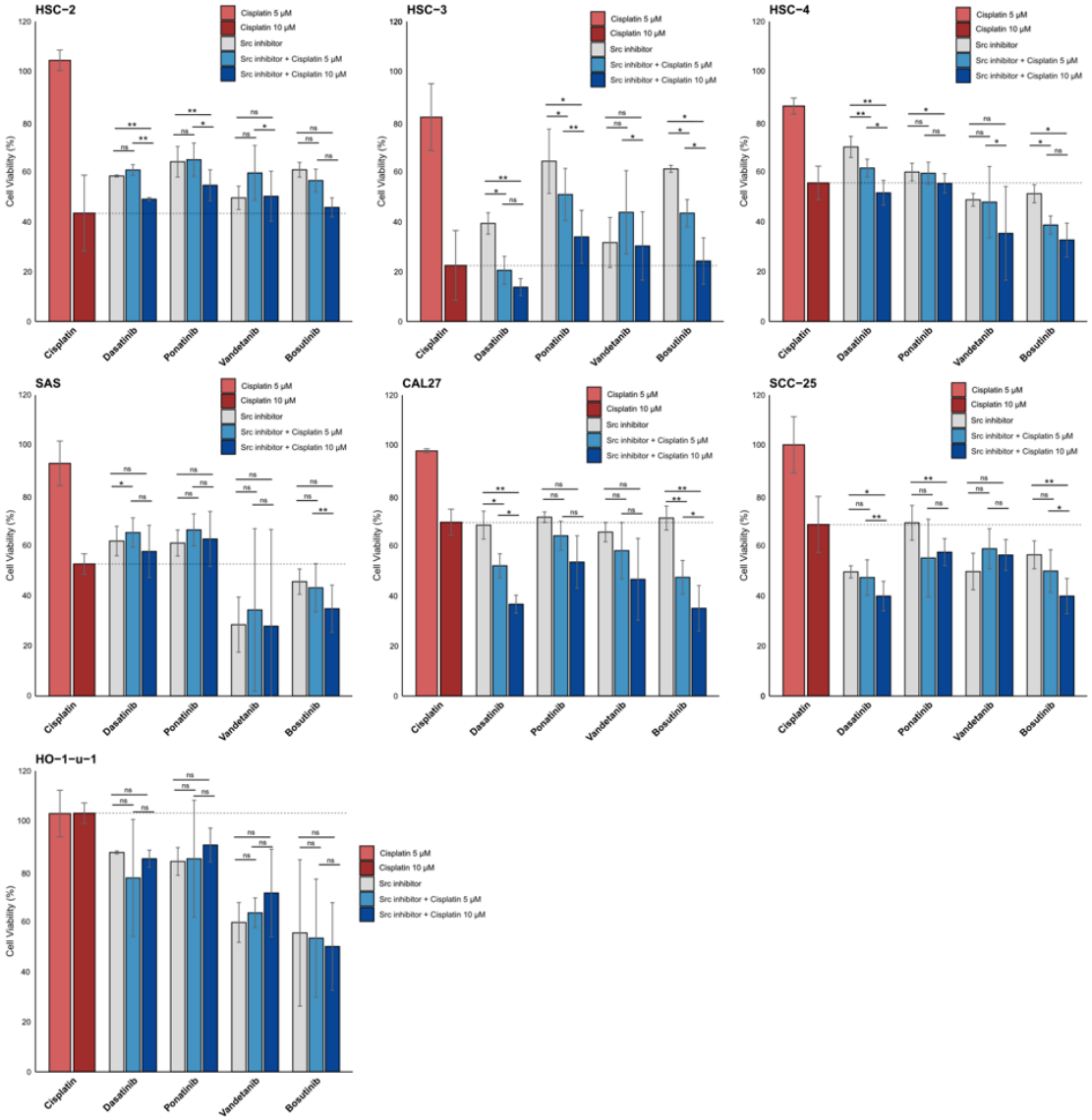

392

393 **Tumor growth inhibition by single treatment of dasatinib and bosutinib *in vivo***

394 Next, we examined whether dasatinib and bosutinib, which showed additive effects *in*
395 *vitro*, could suppress tumor growth as single agents *in vivo* (Fig. 3, Fig. S2, Fig. S3).
396 Since dasatinib and bosutinib demonstrated additive effects with cisplatin in more cell
397 lines than the other Src inhibitors (Fig. 2) and both are relatively inexpensive and thus
398 more suitable for clinical applications; these two inhibitors were selected for further *in*
399 *vivo* analysis. CAL27 cells were selected as the subcutaneous xenograft model because
400 their cells showed reliable tumor formation in preliminary experiments and demonstrated
401 high sensitivity to Src inhibitors with additive effects with cisplatin *in vitro*. To monitor
402 tumor size using *in vivo* imaging system, we established stable Rluc-expressing CAL27
403 (CAL27-Rluc) cells and checked their susceptibility to Src inhibitors (Fig. S1). Src
404 inhibitors suppressed the growth of CAL27-Rluc clones in a similar manner as the CAL27
405 Wt cells. Clone7, which exhibited a median susceptibility to Src inhibitors, was selected
406 for *in vivo* analysis. CAL27-Rluc cells-inoculated BALB/cAJcl nu/nu mice were treated
407 with inhibitors by indicated schedule which were designed to approximate clinically
408 relevant regimens (Fig. 3A). Furthermore, dasatinib (30 mg/kg) and bosutinib (50 mg/kg)
409 were compared in a separate experiment (Fig. S3A). Cisplatin 4 mg/kg was selected as a

410 positive control based on previous reports, and this dose is within the range of the
411 maximum repeated tolerated dose in the mouse model(36).
412 The physical tumor volumes in the cisplatin group at 4 and 2 mg/kg were decreased
413 compared to those in the control group, whereas their size in the dasatinib group continued
414 to increase (Fig 3B). In contrast, IVIS bioluminescence live imaging showed a substantial
415 reduction in the tumor signal in the dasatinib group relative to the control group. In some
416 cases, it exceeded the effect of cisplatin (Fig. 3C, Fig. S2). Body weight gain was
417 impaired in the cisplatin 4 mg/kg group, whereas mice treated with dasatinib or cisplatin
418 (2 mg/kg) maintained stable weight without apparent toxicity (Fig. 3D).
419 Bosutinib treatment led to antitumor activity; one of the three mice died, and the
420 remaining animals showed weight loss, indicating considerable toxicity (Fig. S3B–D).
421 Histological analyses on day 17 showed that tumors from the control and cisplatin groups
422 were solid, well-differentiated squamous cell carcinomas with keratin pearls (Fig. 3E).
423 Contrastingly, tumors from the dasatinib group showed cyst-like structures with hollow
424 interiors and serous fluids. Under magnification, the cells remaining in the lumen had
425 blurred outlines, lost nuclei, and died. In addition, the cancer pearls in the epithelial
426 regions disappeared. In the kidneys, normal kidney structure was maintained in the
427 control group (DMSO) and the dasatinib group. On the other hand, degeneration and

428 atrophy of the renal tubular epithelium and localized rupture were observed in the
429 cisplatin 4 mg/kg group, while only mild renal tubular epithelial atrophy was observed in
430 the cisplatin 2 mg/kg group. These results suggest that renal damage occurred in a dose-
431 dependent manner only in mice treated with cisplatin. The liver tissues retained normal
432 architecture in all groups, corresponding to no apparent tissue damage.
433 Together, these results show that dasatinib exerts antitumor activity *in vivo* by inducing
434 extensive intratumoral cell death, even in cases in which the tumor size appears to
435 increase. Especially, dasatinib achieved tumor suppression that exceeded that by cisplatin
436 under certain conditions, strongly supporting its therapeutic potential. Contrastingly,
437 bosutinib revealed antitumor efficacy comparable to that of cisplatin, but was linked to
438 toxicity, which may limit its clinical utility.

Figure 3 The inhibition of tumor growth by single treatment of Dasatinib in vivo

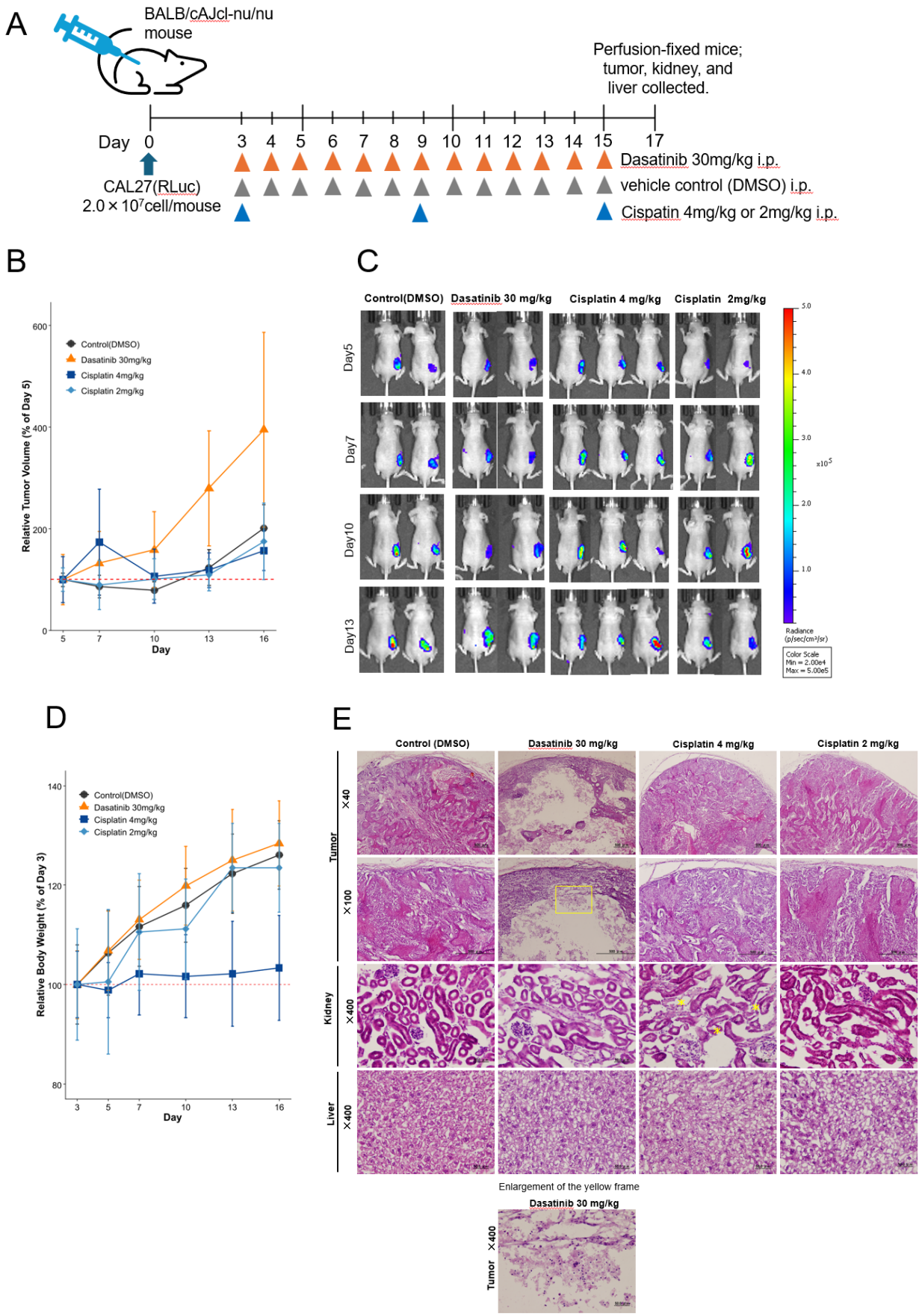

440 **Tumor growth inhibition by the combination treatment of cisplatin and dasatinib *in***

441 ***vivo***

442 We finally evaluated the antitumor efficacy of combination treatment with dasatinib and

443 cisplatin to determine whether the additive effects of Src inhibitors and cisplatin could be

444 reproduced *in vivo*. The dosing schedule was identical to that used for the single-agent

445 treatment (Fig. 3), and mice bearing subcutaneous tumors were assigned to three groups:

446 control, dasatinib 30 mg/kg + cisplatin 4 mg/kg, and dasatinib 30 mg/kg + cisplatin

447 2 mg/kg; Fig. 4A).

448 Tumor volumes in the dasatinib 30 mg/kg + cisplatin 4 mg/kg group showed a slight

449 decrease compared with those in the control group on day 16, whereas tumor size in the

450 dasatinib 30 mg/kg + cisplatin 2 mg/kg group increased relative to the control group and

451 single-agent cisplatin (Fig. 3B, Fig. 4B). Similar to single-agent treatment, tumor volume

452 alone might not completely capture the therapeutic effects of the combination treatment.

453 Thus, we evaluated the tumor burden using IVIS bioluminescence live imaging, which

454 showed substantially decreased tumor signals in both combination groups compared with

455 those in the control group (Fig. 4C, Fig. S4). This finding was consistent with the pattern

456 noted in the dasatinib monotherapy group. Thus, IVIS bioluminescence live imaging on

457 day 13 showed that the antitumor effect of the combination was comparable to the

458 expected additive effect derived from each monotherapy. Body weight in the dasatinib
459 30 mg/kg + cisplatin 4 mg/kg group gradually decreased compared with that in the control
460 group, whereas that in the dasatinib 30 mg/kg + cisplatin 2 mg/kg group slightly increased,
461 especially on days 13 and 16 (Fig. 4D). This suggested that reducing the cisplatin dose
462 may mitigate its toxicity.
463 Histological analysis of the excised tumors showed extensive intratumoral cell death in
464 both combination groups, similar to that noted with dasatinib monotherapy, supporting an
465 antitumor effect that was not reflected by tumor size alone (Fig. 4E). In the kidneys, the
466 dasatinib 30 mg/kg + cisplatin 4 mg/kg group showed tubular epithelial degeneration and
467 atrophy, as well as localized rupture, similar to the cisplatin 4 mg/kg group alone. In the
468 dasatinib 30 mg/kg + cisplatin 2 mg/kg group, only mild tubular epithelial atrophy was
469 observed, like the cisplatin 2 mg/kg group. These results suggest that renal damage occurs
470 in a dose-dependent manner in cisplatin-treated mice, and that concomitant use of
471 dasatinib did not enhance toxicity. Additionally, liver sections revealed no apparent organ
472 toxicity, which is consistent with the results from the single-agent treatment.
473 Collectively, these findings indicate that combination treatment with dasatinib and
474 cisplatin additively improves the antitumor activity *in vivo*. Notably, reducing the

475 cisplatin dose in combination with dasatinib treatment preserved the antitumor efficacy

476 and may help attenuate treatment-related toxicity.

477

Figure 4 The inhibition of tumor growth by combination treatment of Cisplatin and Dasatinib in vivo

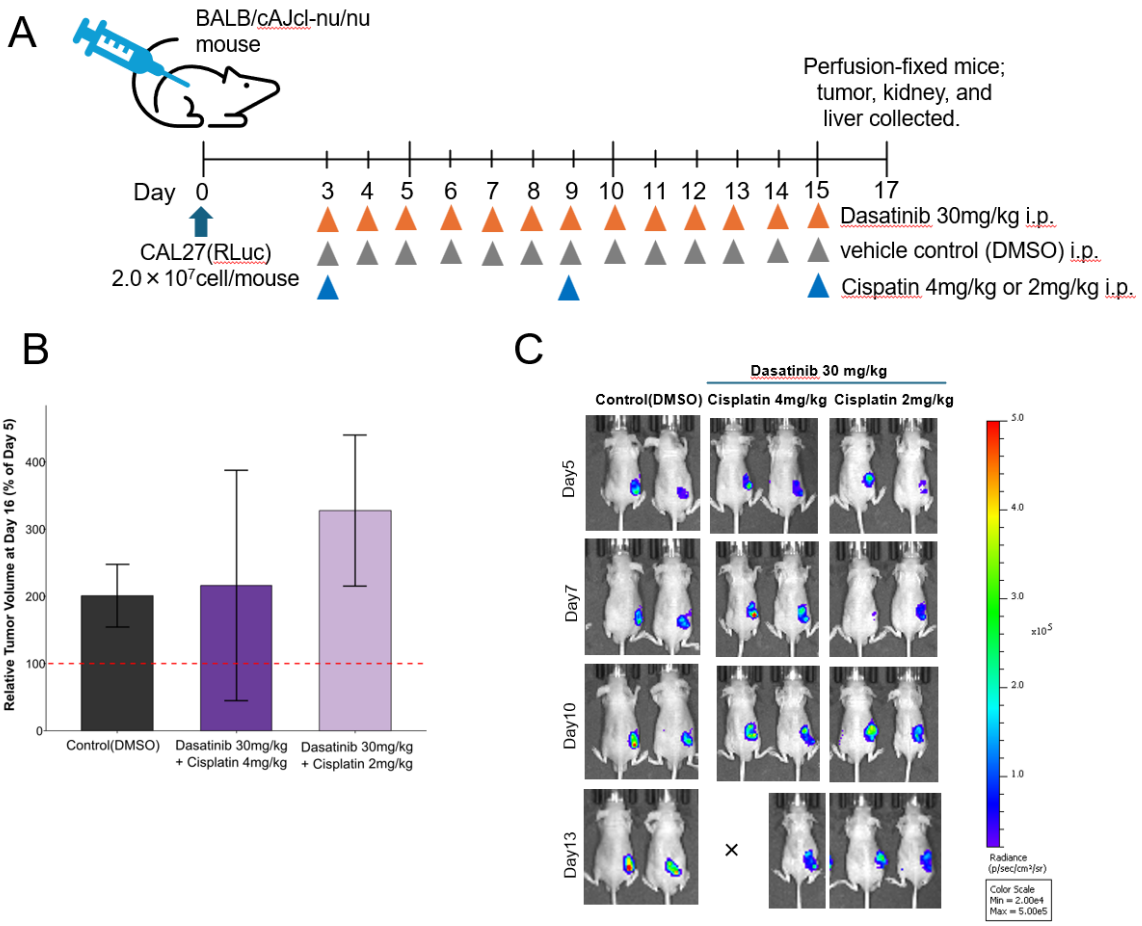

480 **Discussion**

481 Herein, we examined the signaling pathway associated with tumorigenicity in OSCC
482 (Fig. 1A), involvement of Src activity in broad oral cancer cell lines (Fig. 1A and D),
483 sensitivity of OSCC cells to Src inhibitors (Fig. 1B and C, Table-1) and, molecular basis
484 underlying this variability, and the therapeutic effect of combining Src inhibition with
485 cisplatin in *in vitro* and *in vivo* models (Fig. 2 and 4). Particularly, dasatinib showed a
486 distinctive antitumor effect, characterized by extensive intratumoral cell death, leading
487 to a substantial decrease in the tumor burden *in vivo* (Fig. 3E). Additionally, the
488 dasatinib and cisplatin combination markedly decreased tumor volume, even under
489 cisplatin-dose-reduced conditions (Fig. 4), suggesting its potential to maintain antitumor
490 efficacy while mitigating toxicity.

491 OSCC is a molecularly heterogeneous malignancy characterized by aberrant activation
492 of multiple oncogenic signaling pathways, including EGFR, PI3K/AKT/mTOR,
493 JAK/STAT, MET, Wnt/β catenin, and RAS/RAF/MAPK(35). These pathways are
494 closely linked to Src, which serves as a central signaling node that regulates diverse
495 malignant phenotypes. Screening using multiple Src inhibitors showed considerable
496 variability in Src inhibitor sensitivity among the OSCC cell lines (Fig. 1B). This
497 heterogeneity likely reflects the underlying molecular diversity of OSCC and may

498 explain why therapies targeting a single pathway, including the Src pathway, often fail
499 to achieve sufficient efficacy.
500 Previous studies on HNSCC have attributed Src inhibitors' limited efficacy to numerous
501 factors *in vivo*, including the non-lethal nature of Src inhibition in some tumor cells,
502 compensatory activation of alternative pathways such as PI3K/AKT and STAT3(22,26),
503 and differences in EMT status or cell adhesion molecules(27,28). Consistent with these
504 observations, our findings support the notion that the therapeutic response to Src
505 inhibition in OSCC is strongly influenced by molecular diversity. Our data did not
506 support a high phosphorylated-Src/total-Src ratio, although this has been proposed as a
507 predictor of dasatinib sensitivity(30). Although Src activation has been reported in
508 93.75% of OSCC tissues(37), our results suggest that assessing the Src activation status
509 and the degree of downstream pathway suppression are necessary for predicting Src
510 inhibitor sensitivity.
511 An especially striking finding in this study was that dasatinib induced extensive
512 intratumoral cell death *in vivo*, resulting in a considerable decrease in viable tumor
513 mass, even when the overall tumor size remained unchanged or increased (Fig. 3). IVIS
514 data from *in vivo* imaging and histological analyses confirmed a clear dissociation
515 between tumor size and tumor burden, showing an antitumor effect that could not be

516 captured by size-based evaluation alone in some cases. From this perspective, dasatinib
517 showed tumor-suppressive activity comparable to or exceeding that of cisplatin,
518 indicating that the effect underscores its therapeutic potential.
519 Although dasatinib-induced intratumoral cavitation and cell death have not been
520 previously reported, studies on bladder cancer cells have revealed that dasatinib
521 suppresses the phosphorylation of the PI3K/Akt/mTOR pathway and activates
522 apoptosis- and autophagy related proteins(38). These mechanisms may contribute to cell
523 death noted in OSCC. Furthermore, inhibition of angiogenesis may also play a role in
524 necrotic formation because Src activation is necessary for VEGF expression(39).
525 Whether these effects are specific to CAL27 cells or represent a broader OSCC
526 phenotype requires further *in vivo* investigations. Especially, this necrosis-inducing
527 effect was not noted with bosutinib (Fig. S3E). Although this suggests a dasatinib-
528 specific response, the current data are insufficient to determine its specificity, indicating
529 that comparisons with additional Src inhibitors are required.
530 The dasatinib and cisplatin combination markedly decreased the tumor burden, even
531 under cisplatin dose-reduced conditions, indicating its potential to maintain antitumor
532 efficacy while decreasing toxicity (Fig. 4). This combination produced additive rather
533 than synergistic effects *in vitro*, likely reflecting the independent actions of the

534 inhibition of Src downstream signaling by dasatinib and the impairment of DNA repair
535 mechanisms by cisplatin. Despite previous studies have reported that dasatinib
536 suppresses cisplatin-induced Src activation(40) and reverses Src-dependent cisplatin
537 resistance(41), such effects were not noted in the cisplatin-resistant OSCC cell line HO-
538 1-u-1 (Fig. 2E). This may be owing to the Src-independent nature of cisplatin resistance
539 in HO-1-u-1 and its low sensitivity to Src inhibitors. Nevertheless, our results suggest
540 that combining Src inhibitors with cisplatin may enable dose reduction and mitigate
541 toxicity (Fig 2 and 4), offering a clinically meaningful strategy for overcoming
542 resistance and enhancing tolerability.
543 Although bosutinib also showed antitumor activity *in vivo*, its pronounced toxicity,
544 including loss of body weight, may limit its clinical applicability (Fig. S4). The
545 considerable differences in toxicity profiles among the Src inhibitors underscore the
546 criticality of careful drug selection when considering Src-targeted therapies for OSCC.
547 Dasatinib showed a favorable balance between tumor reduction and tolerability,
548 suggesting that it may be a more suitable Src inhibitor for clinical use.
549 This study has some limitations. First, Src inhibitors were ineffective in all the OSCC
550 cell lines, and based on the seven cell lines examined, the molecular determinants of
551 sensitivity could not be conclusively defined. Future studies incorporating a larger and

552 more diverse panel, including patient-derived cell lines, are necessary for identifying the
553 molecular features that predict the responsiveness of the Src inhibitor. Second, complete
554 tumor disappearance could not be confirmed in any of the groups because the endpoint
555 of this study was defined as visible tumor enlargement in mice. Importantly, dasatinib-
556 treated tumors frequently showed extensive central cell death, raising the possibility that
557 they may eventually collapse and regress, even though the time course of this process
558 remains elusive. Further examination is necessary to optimize the combination
559 strategies and treatment schedules. Nonetheless, FDA-approved Src inhibitors are orally
560 administered and are generally less toxic than cytotoxic chemotherapies, leaving
561 considerable room for their clinical application in settings such as neoadjuvant therapy
562 or palliative treatment.
563 In summary, this study reassessed the therapeutic potential of Src inhibition in OSCC
564 and showed that Src inhibitors, especially dasatinib, are promising candidates, both as
565 monotherapy and in combination with cisplatin. Dasatinib's ability to decrease tumor
566 burden and the potential for toxicity reduction through a reduction in cisplatin dose
567 provide a foundation for developing new therapeutic strategies aimed at expanding
568 treatment options and enhancing outcomes in patients with OSCC. Thus, our results

569 provide new insights that may allow the establishment of future therapeutic strategies

570 for oral cancer.

571

Acknowledgements

We thank all of our laboratory members, especially Akemi Takada, who supported the handling of our budgets. This work was supported by AMED under Grant Number, JP23bm1323001, JMU Graduate Student Start-Up Award, and JST SPRING, Grant Number JPMJSP2183.

Author Contributions

K.O. conceived and designed the study. Y.O. performed all the experiments and analyzed the data. Y.O. and K.O. interpreted experimental results. Y.O. and K.O. wrote the manuscript. Y.O., T.N., H.M., and K.O. edited the manuscript. All the authors have reviewed and approved the final manuscript.

Competing Interests

The authors declare no competing interests.

Data Availability Statement

The authors declare that the data supporting the findings of this study are available in the article and its Supplementary Information files. All relevant data are available from the authors upon reasonable request.

References

1. Rumgay H, Colombet M, Ramos da Cunha A, Filho AM, Warnakulasuriya S, Conway DI, et al. Global incidence of lip, oral cavity, and pharyngeal cancers by subsite in 2022. CA Cancer J Clin [Internet]. 2026. Available from: https://www.ncbi.nlm.nih.gov/pubmed/41335400

2. Cancer Today [Internet]. [cited 2026 Mar 3]. Available from: https://gco.iarc.who.int/today/

3. Chow LQM. Head and Neck Cancer. Reply. N Engl J Med. 2020. p. e57.

4. Liu F, Chen F, Huang J, Yan L, Wu J, Qiu Y, et al. Prospective study on factors affecting the prognosis of oral cancer in a Chinese population. Oncotarget. 2017. p. 4352–9.

5. Kim MJ, Ahn KM. Prognostic factors of oral squamous cell carcinoma: the importance of recurrence and pTNM stage. Maxillofac Plast Reconstr Surg. 20240304th ed. 2024. p. 8.

6. Leemans CR, Braakhuis BJ, Brakenhoff RH. The molecular biology of head and neck cancer. Nat Rev Cancer. 20101216th ed. 2011. p. 9–22.

7. Mäkitie AA, Alabi RO, Pulkki-Råback L, Almangush A, Beitler JJ, Saba NF, et al. Psychological Factors Related to Treatment Outcomes in Head and Neck Cancer. Adv Ther. 20240807th ed. 2024. p. 3489–519.

8. Blatt S, Krüger M, Sagheb K, Barth M, Kämmerer PW, Al-Nawas B. Tumor Recurrence and Follow-Up Intervals in Oral Squamous Cell Carcinoma. J Clin Med [Internet]. 20221129th ed. 2022. Available from: https://www.ncbi.nlm.nih.gov/pubmed/36498636

9. Ghanaati S, Udeabor SE, Winter A, Sader R, Heselich A. Cancer Recurrence in Operated Primary Oral Squamous Cell Carcinoma Patients Seems to Be Independent of the Currently Available Postoperative Therapeutic Approach: A Retrospective Clinical Study. Curr Oncol [Internet]. 20250401st ed. 2025. Available from: https://www.ncbi.nlm.nih.gov/pubmed/40277765

10. Slieker FJB, Rombout DAA, de Bree R, Van Cann EM. Local recurrence and survival after treatment of oral squamous cell carcinoma of the maxilla: A systematic review and meta-analysis. Oral Surg Oral Med Oral Pathol Oral Radiol. 20211013th ed. 2022. p. 626–38.

11. Lefebvre JL. Current clinical outcomes demand new treatment options for SCCHN. Ann Oncol. 2005. p. vi7–12.

12. Rabik CA, Dolan ME. Molecular mechanisms of resistance and toxicity associated with platinating agents. Cancer Treat Rev. 20061103rd ed. 2007. p. 9–23.

13. Atashi F, Vahed N, Emamverdizadeh P, Fattahi S, Paya L. Drug resistance against 5-fluorouracil and cisplatin in the treatment of head and neck squamous cell carcinoma: A systematic review. J Dent Res Dent Clin Dent Prospects. 20210825th ed. 2021. p. 219–25.

14. Lokich J, Anderson N. Carboplatin versus cisplatin in solid tumors: an analysis of the literature. Ann Oncol. 1998. p. 13–21.

15. Gebre-Medhin M, Adrian G, Engström P, Cange HH, Hammarstedt-Nordenvall L, Reizenstein J, et al. Chemoradiation therapy With Cisplatin Versus Cetuximab in Patients With Locoregionally Advanced Head and Neck Squamous Cell Cancer-Mature Results of the ARTSCAN III Trial. Int J Radiat Oncol Biol Phys. 20250619th ed. 2025. p. 681–90.

642 16. Ferris RL, Blumenschein G, Fayette J, Guigay J, Colevas AD, Licitra L, et al.
643 Nivolumab for Recurrent Squamous-Cell Carcinoma of the Head and Neck. N Engl
644 J Med. 20161008th ed. 2016. p. 1856–67.

645 17. Larkins E, Blumenthal GM, Yuan W, He K, Sridhara R, Subramaniam S, et al. FDA
646 Approval Summary: Pembrolizumab for the Treatment of Recurrent or Metastatic
647 Head and Neck Squamous Cell Carcinoma with Disease Progression on or After
648 Platinum-Containing Chemotherapy. Oncologist. 20170522nd ed. 2017. p. 873–8.

649 18. Irby RB, Yeatman TJ. Role of Src expression and activation in human cancer.
650 Oncogene. 2000. p. 5636–42.

651 19. Aleshin A, Finn RS. SRC: a century of science brought to the clinic. Neoplasia.
652 2010. p. 599–607.

653 20. Mandal M, Myers JN, Lippman SM, Johnson FM, Williams MD, Rayala S, et al.
654 Epithelial to mesenchymal transition in head and neck squamous carcinoma:
655 association of Src activation with E-cadherin down-regulation, vimentin expression,
656 and aggressive tumor features. Cancer. 2008. p. 2088–100.

21. Cheng SJ, Kok SH, Lee JJ, Yen-Ping Kuo M, Cheng SL, Huang YL, et al. Significant association of SRC protein expression with the progression, recurrence, and prognosis of oral squamous cell carcinoma in Taiwan. Head Neck. 20111102nd ed. 2012. p. 1340–5.

22. Yang Z, Liao J, Cullen KJ, Dan H. Inhibition of IKKβ/NF-κB signaling pathway to improve Dasatinib efficacy in suppression of cisplatin-resistant head and neck squamous cell carcinoma. Cell Death Discov. 20200515th ed. 2020. p. 36.

23. Ammer AG, Kelley LC, Hayes KE, Evans JV, Lopez-Skinner LA, Martin KH, et al. Saracatinib Impairs Head and Neck Squamous Cell Carcinoma Invasion by Disrupting Invadopodia Function. J Cancer Sci Ther. 2009. p. 52–61.

24. Brooks HD, Glisson BS, Bekele BN, Johnson FM, Ginsberg LE, El-Naggar A, et al. Phase 2 study of dasatinib in the treatment of head and neck squamous cell carcinoma. Cancer. 20101129th ed. 2011. p. 2112–9.

25. Fury MG, Baxi S, Shen R, Kelly KW, Lipson BL, Carlson D, et al. Phase II study of saracatinib (AZD0530) for patients with recurrent or metastatic head and neck squamous cell carcinoma (HNSCC). Anticancer Res. 2011 Jan;31(1):249–53.

673 26. Sen B, Saigal B, Parikh N, Gallick G, Johnson FM. Sustained Src inhibition results
674 in signal transducer and activator of transcription 3 (STAT3) activation and cancer
675 cell survival via altered Janus-activated kinase-STAT3 binding. Cancer Res.
676 20090217th ed. 2009. p. 1958–65.

677 27. Lee S, Park S, Ryu JS, Kang J, Kim I, Son S, et al. c-Src inhibitor PP2 inhibits head
678 and neck cancer progression through regulation of the epithelial-mesenchymal
679 transition. Exp Biol Med (Maywood). 20221217th ed. 2023. p. 492–500.

680 28. Ortiz MA, Mikhailova T, Li X, Porter BA, Bah A, Kotula L. Src family kinases,
681 adaptor proteins and the actin cytoskeleton in epithelial-to-mesenchymal transition.
682 Cell Commun Signal. 20210630th ed. 2021. p. 67.

683 29. Wu Z, Doondeea JB, Gholami AM, Janning MC, Lemeer S, Kramer K, et al.
684 Quantitative chemical proteomics reveals new potential drug targets in head and
685 neck cancer. Mol Cell Proteomics. 20110928th ed. 2011. p. M111.011635.

686 30. Levitt JM, Yamashita H, Jian W, Lerner SP, Sonpavde G. Dasatinib is preclinically
687 active against Src-overexpressing human transitional cell carcinoma of the
688 urothelium with activated Src signaling. Mol Cancer Ther. 20100420th ed. 2010. p.
689 1128–35.

31. Wang H, Lu Y, Wang M, Shen A, Wu Y, Xu X, et al. Src inhibitor dasatinib sensitized gastric cancer cells to cisplatin. Med Oncol. 20221216th ed. 2022. p. 49.

32. Futami M, Sato K, Miyazaki K, Suzuki K, Nakamura T, Tojo A. Efficacy and Safety of Doubly-Regulated Vaccinia Virus in a Mouse Xenograft Model of Multiple Myeloma. Mol Ther Oncolytics. 20170722nd ed. 2017. p. 57–68.

33. Hanahan D, Weinberg RA. The hallmarks of cancer. Cell. 2000. p. 57–70.

34. Zhou Y, Wang L, Liu M, Jiang H, Wu Y. Oral squamous cell carcinoma: Insights into cellular heterogeneity, drug resistance, and evolutionary trajectories. Cell Biol Toxicol. 20250612th ed. 2025. p. 101.

35. Tan Y, Wang Z, Xu M, Li B, Huang Z, Qin S, et al. Oral squamous cell carcinomas: state of the field and emerging directions. Int J Oral Sci. 20230922nd ed. 2023. p. 44.

36. Perše M. Cisplatin Mouse Models: Treatment, Toxicity and Translatability. Biomedicines. 2021 Oct 7;9(10):1406. doi:10.3390/biomedicines9101406 PubMed PMID: 34680523; PubMed Central PMCID: PMC8533586.

705 37. Theocharis S, Klijanienko J, Giaginis C, Alexandrou P, Patsouris E, Sastre-Garau X.
706 FAK and Src expression in mobile tongue squamous cell carcinoma: associations
707 with clinicopathological parameters and patients survival. J Cancer Res Clin Oncol.
708 20120410th ed. 2012. p. 1369–77.

709 38. Ho JN, Byun SS, Kim D, Ryu H, Lee S. Dasatinib induces apoptosis and autophagy
710 by suppressing the PI3K/Akt/mTOR pathway in bladder cancer cells. Investig Clin
711 Urol. 2024. p. 593–602.

712 39. Gray MJ, Zhang J, Ellis LM, Semenza GL, Evans DB, Watowich SS, et al. HIF-
713 1alpha, STAT3, CBP/p300 and Ref-1/APE are components of a transcriptional
714 complex that regulates Src-dependent hypoxia-induced expression of VEGF in
715 pancreatic and prostate carcinomas. Oncogene. 2005. p. 3110–20.

716 40. Ceppi P, Papotti M, Monica V, Lo Iacono M, Saviozzi S, Pautasso M, et al. Effects
717 of Src kinase inhibition induced by dasatinib in non-small cell lung cancer cell lines
718 treated with cisplatin. Mol Cancer Ther. 20091027th ed. 2009. p. 3066–74.

719 41. Masumoto N, Nakano S, Fujishima H, Kohno K, Niho Y. v-src induces cisplatin
720 resistance by increasing the repair of cisplatin-DNA interstrand cross-links in
721 human gallbladder adenocarcinoma cells. Int J Cancer. 1999. p. 731–7.

722

723 **Figure Legends**

724 **Figure 1 Src activity and its inhibitory effect of tumor growth by specific inhibitors**

725 **in different oral cancer cell lines**

726 **A** Western blot analysis of the oral squamous carcinoma cell lines to monitor numerous

727 signaling pathways. The phosphorylated and total protein levels were determined as

728 indicated. **B** Cell viability (%) of the oral squamous carcinoma cell lines treated with

729 each Src inhibitor for 72 h. Viability was measured using CellTiter-Glo, and values are

730 indicated relative to the 1% dimethyl sulfoxide (DMSO) control. Data represent

731 mean ± standard deviation from three independent experiments (n = 3). **C** IC_{50} curves of

732 the oral squamous carcinoma cell lines treated with each Src inhibitor for 36 h. Viability

733 was measured using CellTiter-Glo and normalized to that of the 1% DMSO control.

734 Values represent the mean of n = 3. **D, E** Western blot analysis of the oral squamous

735 carcinoma cell lines to investigate Src (D) and MAPK (E) activity induced by different

736 Src inhibitors. Oral squamous carcinoma cell lines were treated with an Src inhibitor for

737 18 h, followed by western blot analysis. D indicates the Src phosphorylation (Tyr416),

738 and E reveals MAPK pathway-related proteins. Supplementary Table S1 lists the

739 concentrations of the Src inhibitors used.

740

741 **Figure 2 The tumor inhibitory effect by combination therapy using cisplatin and**

742 **Src inhibitor.**

743 Cells were treated with cisplatin (10 μM or 5 μM), each Src inhibitor (dasatinib, ponatinib,

744 vandetanib, or bosutinib) alone, or their combinations for 36 h. Cell viability is indicated

745 as the percentage relative to the 1% dimethyl sulfoxide (DMSO) control. Data represent

746 mean ± standard deviation from three independent experiments. A–G show the data for

747 the indicated cells. P-values were calculated using paired t-tests in Microsoft Excel.

748 Statistical significance was indicated as $p < 0.01$ **, $p < 0.05$ *, and $p \geqq 0.05$ ns.

749

750 **Figure 3 Tumor growth inhibition by single treatment of dasatinib *in vivo*.**

751 **A** Experimental schedule for a single treatment with dasatinib *in vivo*. RLuc-expressing

752 CAL27 (CAL27-Rluc) cells (clone 7) (2×10^7 cells/mouse) were subcutaneously

753 implanted into the right flank of 5-week-old male BALB/cAJcl nu/nu mice. Three days

754 following implantation, the mice were randomly assigned to four treatment groups:

755 vehicle control (dimethyl sulfoxide [DMSO]), dasatinib alone (30 mg/kg), cisplatin alone

756 (4 mg/kg), and cisplatin alone (2 mg/kg).(n=5–6). **B** Tumor volumes in each time point

757 (mean ± s.d., n = 5–6). Tumor volumes were measured using calipers and calculated as L

758 × W^2 × 0.52. Measurements were conducted every 2 to 3 days. The tumor volumes were
759 normalized to the volume on day 5 for each mouse. **C** IVIS bioluminescence live imaging
760 of the tumor burden (additional mice are indicated in Fig. S2). Bioluminescence signals
761 were quantified 10 min following ViviRen injection according to the manufacturer's
762 instructions. D Body weights of nude mice from various treatment regimens implanted
763 with CAL27-Rluc xenografts. Dasatinib was intraperitoneally administered at 30 mg/kg
764 once daily and cisplatin was intraperitoneally administered at 4 or 2 mg/kg once weekly
765 for two consecutive weeks. Body weights are presented as mean ± standard deviation (n
766 = 5–6) and were normalized to the weight on Day 3 for each mouse. **E** Hematoxylin and
767 eosin staining of the tumor, kidney, and liver sections. Mice were perfusion-fixed on
768 day 17 and the harvested tissues were processed to generate frozen sections for
769 histological analysis. Representative images of each organ are presented. Tumor
770 histology: Control (DMSO) and cisplatin groups showed solid squamous cell carcinoma.
771 Dasatinib group exhibited a hollow, cyst-like structure with evidence of cell death within
772 the lumen. Kidney histology: Control (DMSO) and dasatinib groups displayed normal
773 renal architecture. Cisplatin 4 mg/kg group caused tubular epithelial degeneration and
774 atrophy with focal rupture (*), while cisplatin 2 mg/kg groups induced mild tubular
775 epithelial atrophy. Liver histology: All groups showed normal hepatic morphology

776 without detectable abnormalities. Scale bars: 500 μm (×40, ×100); 50 μm (×400).

777

778 **Figure 4 Tumor growth inhibition by combination treatment of cisplatin and**

779 **dasatinib *in vivo***

780 **A** Experimental schedule for the combination treatment with dasatinib and cisplatin *in*

781 *vivo*. CAL27-Rluc cells (clone 7) (2×10^7 cells per mouse) were subcutaneously

782 implanted into the right flank of 5-week-old male BALB/cAJcl nu/nu mice. Three days

783 following implantation, the mice were randomly assigned to three treatment groups:

784 vehicle control (dimethyl sulfoxide [DMSO]), dasatinib (30 mg/kg) plus cisplatin

785 (4 mg/kg), and dasatinib (30 mg/kg) plus cisplatin (2 mg/kg). (n=5–6). **B** Tumor

786 volumes normalized to Day 3 at the final Day 16 time point (mean ±standard deviation

787 (s.d.), n = 5–6). Tumor volumes were measured using calipers and calculated as $L \times W^2$

788 × 0.52. Measurements were conducted every 2 to 3 days. **C** IVIS bioluminescence live

789 imaging of the tumor burden (additional mice are illustrated in Fig. S2).

790 Bioluminescence signals were quantified 10 min following ViviRen injection according

791 to the manufacturer's instructions. **D** Body weight of nude mice normalized to Day 3 at

792 the final Day 16 time point (mean ± s.d., n = 5–6). **E** Hematoxylin and eosin staining of

793 the tumor, kidney, and liver sections. Mice were perfusion-fixed on day 17 and

794 harvested tissues were processed to generate frozen sections for histological analysis.
795 Representative images of each organ are indicated. Tumor histology: Control group
796 showed solid squamous cell carcinoma. Dasatinib + cisplatin 4 mg/kg and dasatinib +
797 cisplatin 2 mg/kg group exhibited a hollow, cyst-like structure with evidence of cell
798 death within the lumen. Kidney histology: Control (DMSO) group displayed normal
799 renal architecture. dasatinib + cisplatin 4 mg/kg group caused tubular epithelial
800 degeneration and atrophy with focal rupture (*), while dasatinib + cisplatin 2 mg/kg
801 groups induced mild tubular epithelial atrophy. Liver histology: All groups showed
802 normal hepatic morphology without detectable abnormalities. Scale bars: 500 μm (×40,
803 ×100); 50 μm (×400).
804

805 **Supplementary Figures and tables**

806

807 **Supplementary Table 1.**

808 **Concentrations of Src inhibitors used for the Western blot analyses.**

	Dasatinib	Ponatinib	Vandetanib	Bosutinib
HSC-2	**20 μM**	**5 μM**	**10 μM**	**9 μM**
HSC-3	**10 μM**	**2 μM**	**10 μM**	**10 μM**
HSC-4	**40 μM**	**7 μM**	**30 μM**	**15 μM**
SAS	**40 μM**	**10 μM**	**40 μM**	**15 μM**
Ho-1-u-1	**70 μM**	**9 μM**	**30 μM**	**30 μM**
CAL27	**15 μM**	**7 μM**	**15 μM**	**10 μM**
SCC-25	**10 μM**	**3 μM**	**10 μM**	**10 μM**

809

810

811 **Supplementary Table 2.**

812 **Concentrations of Src inhibitors used for the cell viability and combination**

813 **treatment assays.**

	Dasatinib	Ponatinib	Vandetanib	Bosutinib
HSC-2	**0.1 μM**	**2 μM**	**5 μM**	**5 μM**
HSC-3	**10 μM**	**2 μM**	**8 μM**	**5 μM**
HSC-4	**10 μM**	**5 μM**	**25 μM**	**15 μM**
SAS	**10 μM**	**5 μM**	**50 μM**	**25 μM**
Ho-1-u-1	**10 μM**	**5 μM**	**25 μM**	**25 μM**
CAL27	**10 μM**	**5 μM**	**10 μM**	**10 μM**
SCC-25	**10 μM**	**2 μM**	**8 μM**	**10 μM**

814

815

Supplementary Figure 1 Comparison of drug sensitivity in RLuc-labeled CAL27 bulk cells and clones 1–7 using CellTiter-Glo and EnduRen assays.

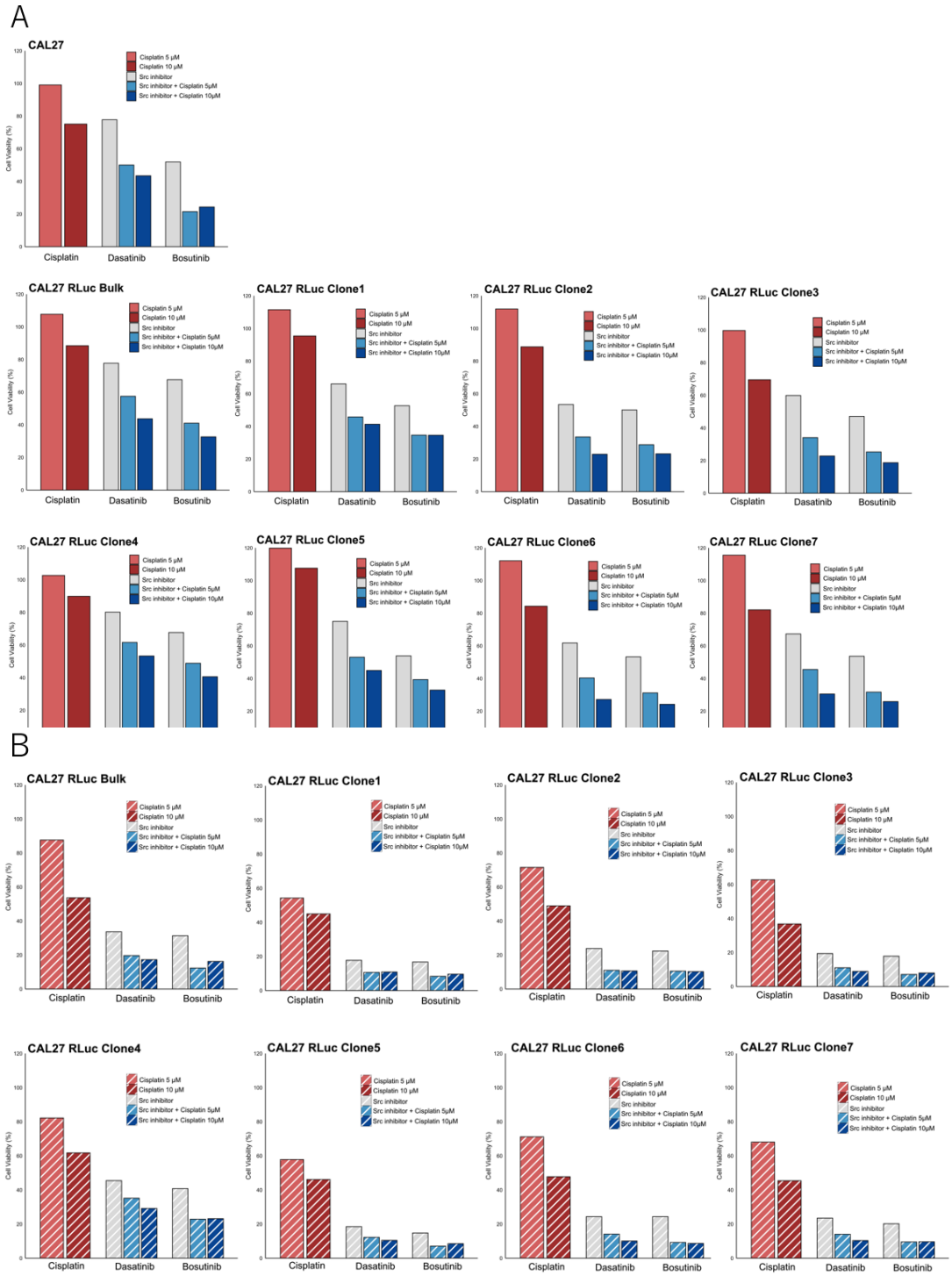

819 Drug sensitivity of stable Renilla luciferase (Rluc)-expressing CAL27 (CAL27-Rluc)

820 bulk cells and clones 1–7 was evaluated 36 h following treatment using CellTiter-Glo

821 (A) and EnduRen (B) assays.

822

823

Supplementary Figure 2 Supplementary IVIS bioluminescence images corresponding to Fig. 3

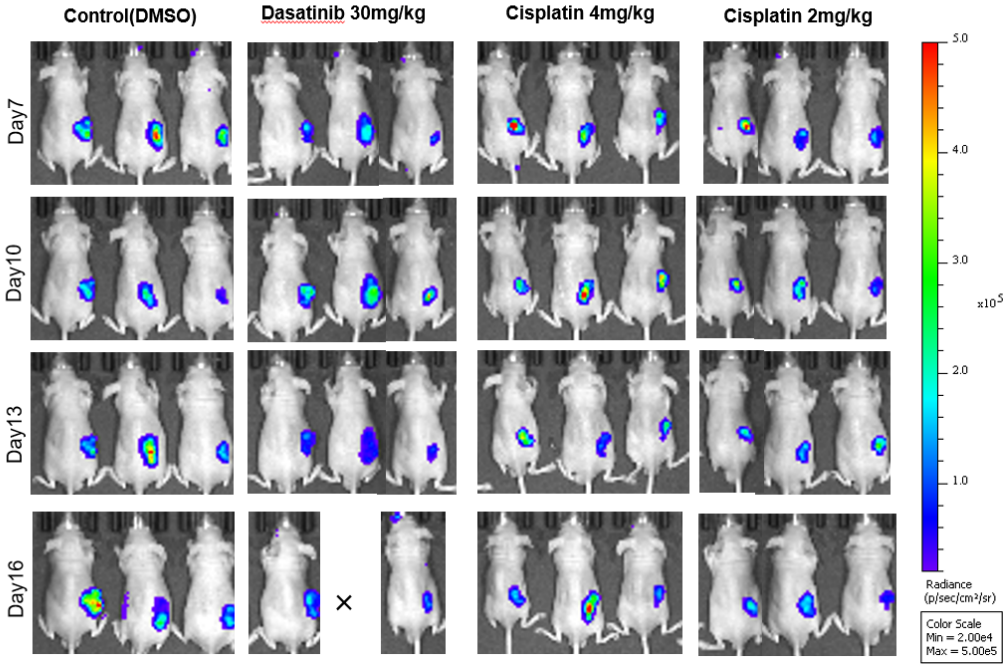

Additional IVIS bioluminescence live images corresponding to Fig. 3. These images include mice scanned at various time points, which are not indicated in the main figure but contribute to the total sample size (n = 5–6). One of three mice in the dasatinib group died on day 16.

Supplementary Figure 3 Tumor growth inhibition by single treatment of dasatinib and bosutinib *in vivo*

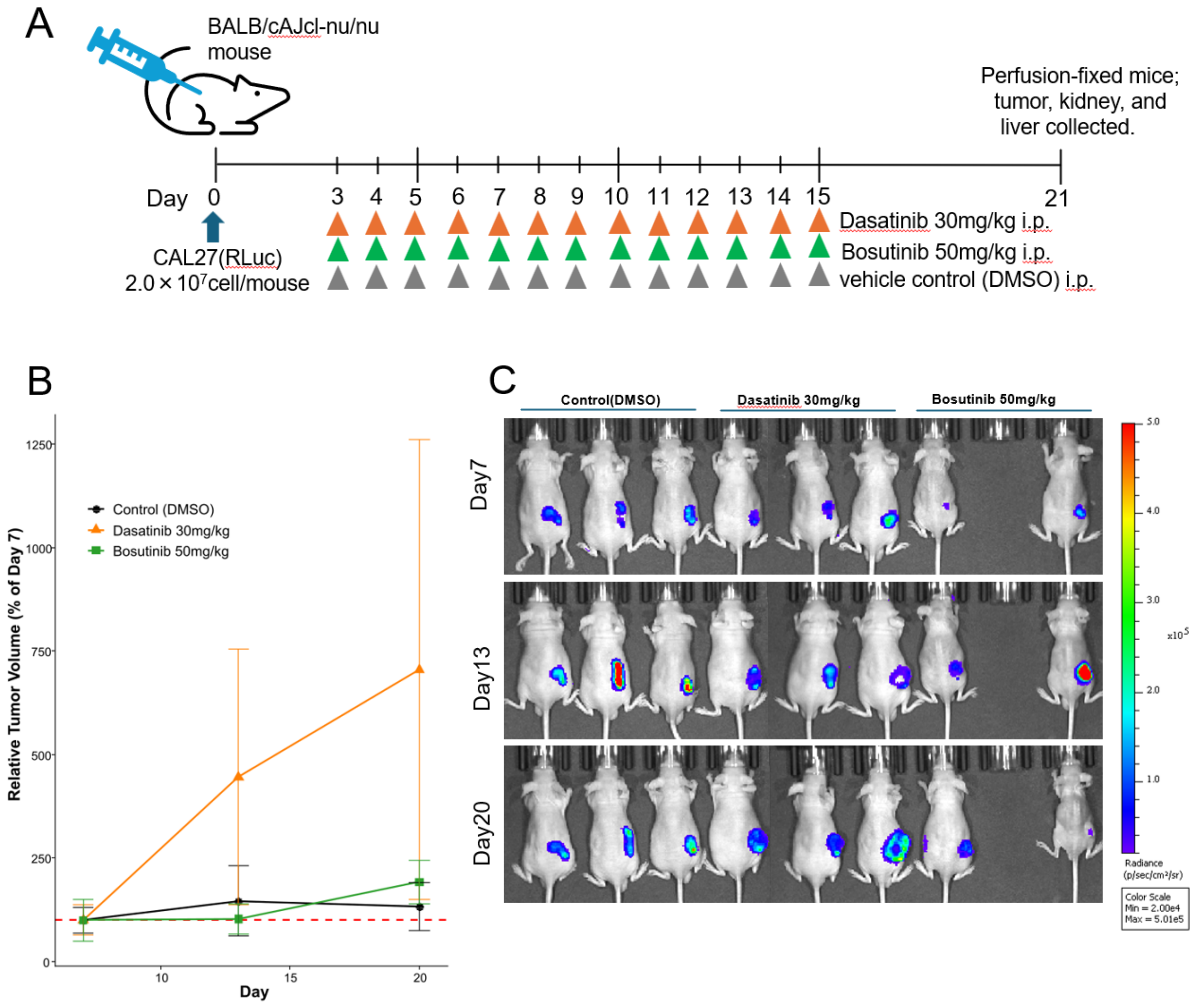

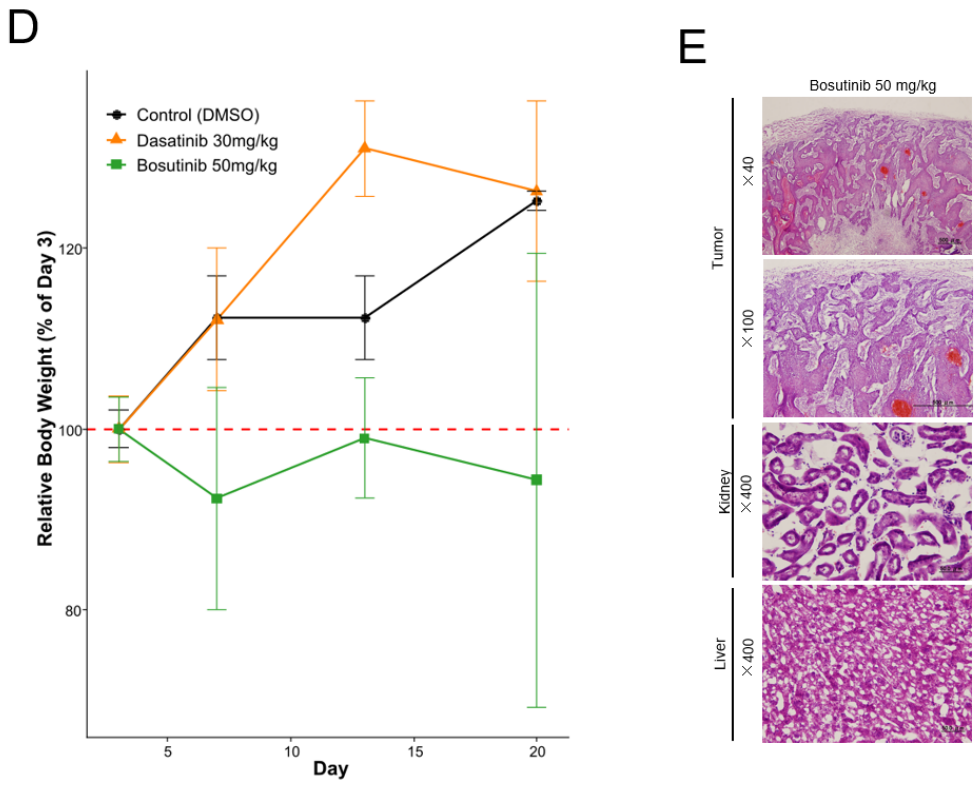

836 **A** Experimental schedule for single treatment with dasatinib and bosutinib *in vivo*.

837 CAL27-Rluc cells (clone 7) (2×10^7 cells/mouse) were subcutaneously implanted into

838 the right flank of 5-week-old male BALB/cAJcl nu/nu mice. Three days following

839 implantation, the mice were randomly assigned to four treatment groups: vehicle control

840 (dimethyl sulfoxide [DMSO]), dasatinib alone (30 mg/kg), and bosutinib alone

841 (50 mg/kg). Dasatinib, bosutinib, and DMSO were dissolved in 10 mM Tris-HCl

842 (pH 7.4). All drugs were intraperitoneally administered at a volume of 100 µL per

843 mouse. Dasatinib, bosutinib, and DMSO were administered once daily (n=3). **B** Tumor

844 volumes normalized to Day 7 at the final Day 20 time point (mean ± standard deviation

845 [s.d.], n = 2–3). Tumor volumes were measured using calipers and calculated as $L \times W^2$

× 0.52. Measurements were conducted every 2–3 days. **C** IVIS bioluminescence live imaging of tumor burden. One of three mice in the bosutinib group died on day 6. **D** Body weights of nude mice from various treatment regimens implanted with CAL27-Rluc xenografts. Body weights are presented as mean ± standard deviation [s.d.] (n = 5–6) and were normalized to the wight on Day 3 for each mouse.(mean ± s.d., n = 2–3). **E** Hematoxylin and eosin staining of the tumor, kidney, and liver sections. Mice were perfusion-fixed on day 21 and the harvested tissues were processed to generate frozen sections for histological analysis. Representative images of each organ are presented. Tumor histology: Bosutinib group showed solid squamous cell carcinoma. Kidney histology: Bosutinib group displayed normal renal architecture. Liver histology: Bosutinib group showed normal hepatic morphology without detectable abnormalities. Scale bars: 500 μm (×40, ×100); 50 μm (×400).

859 **Supplementary Figure 4 Supplementary IVIS bioluminescence images**

860 **corresponding to Fig. 4**

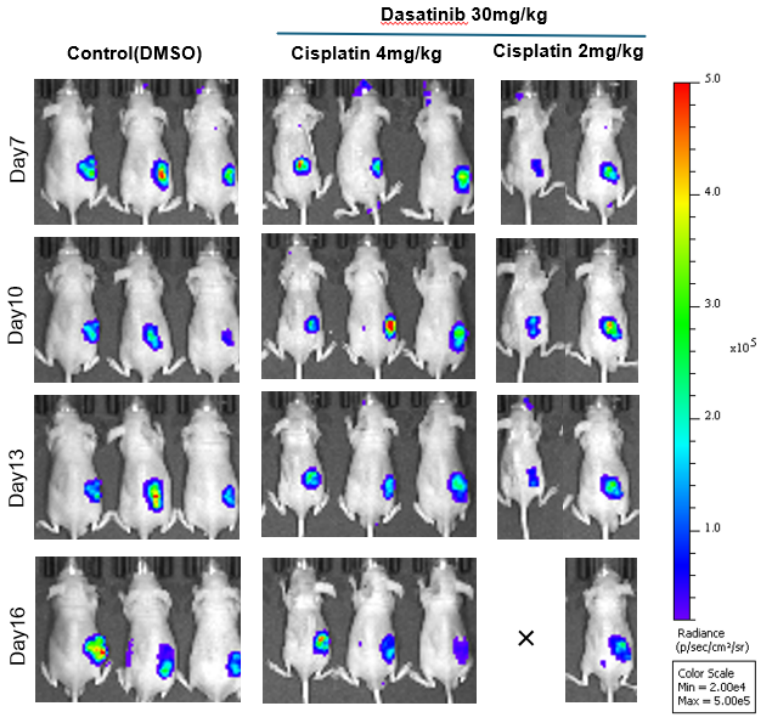

861

862 Additional IVIS bioluminescence live images corresponding to Fig. 4. These images

863 included mice scanned at various time points, which were not included in the main figure

864 but contributed to the total sample size (n = 5–6). One of three mice in the dasatinib

865 30 mg/kg + cisplatin 2 mg/kg group died on day 14.

866